Freeze-drying and hot-pressing strategy to embed two-dimensional $Ti_{0.87}O_2$ monolayers in commercial polypropylene films with enhanced dielectric properties

Wenchao Tian
Fudan University
Cailing Cai
Fudan University
Zeyi Wu
Fudan University
Chenchen Zhang
State Grid Anhui Electric Power Company
Ting Yin
China Electric Power Research Institute
Sijia Lao
China Electric Power Research Institute
Fei Yan
China Electric Power Research Institute
Hu linfeng (linfenghu@fudan.edu.cn)
Fudan University https://orcid.org/0000-0002-0640-508X

Rapid Communication

Keywords: Ti0.87O2 nanosheets, polypropylene, freeze-drying; surface functionalization, hot pressing, dielectric constant

Posted Date: November 5th, 2020

DOI: https://doi.org/10.21203/rs.3.rs-59737/v2

Version of Record: A version of this preprint was published at Journal of Advanced Ceramics on February 5th, 2021. See the published version at https://doi.org/10.1007/s40145-020-0443-0.

Abstract

The dielectric capacitor has been widely used in advanced electronic and electrical power systems due to their capability of ultrafast charging-discharging and ultrahigh power density. Nevertheless, their energy density is still limited by the low dielectric constant (≈ 2.2) of the commercial dielectric polypropylene (PP). The conventional enhancement strategy by embedding inorganic fillers in PP matrix is still difficult and challenging due to that PP hardly dissolves in any inorganic/organic solvent. In this work, we develop a new strategy including freeze-drying, surface functionalization and hot-pressing to incorporate $Ti_{0.87}O_2$ monolayers in PP film. A series of uniform composited $Ti_{0.87}O_2$@PP film has been successfully fabricated with $Ti_{0.87}O_2$ content range of 0-15 wt%. The maximum dielectric constant of the as-prepared $Ti_{0.87}O_2$@PP film is 3.27 when the $Ti_{0.87}O_2$ content is 9 wt%, which is about 1.5 times higher than that of pure PP. Our study provides a feasible strategy to embed two-dimensional material into commercial PP thin-film with superior dielectric performance for practical application.

1. Introduction

Recently, electrical energy storage devices have been attracting immense research interest with the worldly growing demand for energy requirement [1-3]. Dielectric capacitors play an important role in ultrafast charge-discharge capability, which are desired for a broad range of application such as hybrid electrical vehicles (HEVs), pulse power weapon and grid systems [4-7]. However, their energy density is still much lower than those of electrochemical devices including batteries and supercapacitors. Known that the commercial dielectric capacitors constructed from biaxially oriented polypropylene (PP) thin-films just show insufficient energy density of 1.2 J/cm at 640 MV/m with the low dielectric constant (ε_r = 2.2), severely limiting their potential applications on HEVs and grid systems [8, 9].

In principle, the energy density (W) of dielectric capacitors is determined by the applied electric field (E) and dielectric constant (ε_r) as

$$W = \varepsilon_0 \varepsilon_r E^2/2$$

Wherein ε_0 is the vacuum permittivity (8.85×10^{-12} F/m). Theoretically, improving dielectric constant (ε_r) is a very effective route to gain high energy density. Note that ceramics show high dielectric constant but low breakdown strength while polymers exhibit high breakdown strength but low dielectric constant. During the past decades, a lot of researches have been carried out on introducing ceramics nanofillers into polymer matrix for polymer/inorganic composites to realize the optimized dielectric properties.

Two-dimensional (2D) oxide nanosheets, which possess atomic or molecular thickness and infinite planar dimensions, have been attracting remarkable interests on energy storage fields due to their ultrahigh specific surface area, excellent mechanical flexibility and even quantum confinement. Typically, $Ti_{0.87}O_2$ atomic monolayer has been considered as a novel high-κ compound with a layered crystallographic structure in which TiO_6 octahedra are edge-linked in a lepidocrocite-type 2D lattice.

Previous experimental investigations demonstrate that a multilayer thin-film constructed from $Ti_{0.87}O_2$ nanosheets as building blocks on solid-state $SrRuO_3$ substrate exhibit a high dielectric constant of ~125 when the thicknesses down to 10 nm [10]. Such a dielectric constant is much larger than that of anatase (ε_r = 30-40) and rutile TiO_2 (ε_r = 80-100) [11]. The excellent high-κ behavior should be originated from the existence of abundant Ti vacancies rather than oxygen vacancies which act as carrier traps and high-leakage paths.

Motivated by these intrinsic merits, incorporation of oxide nanosheets into polymer matrix to form polymer nanocomposites has recently emerged as a very promising strategy to realize the dielectric thin-film with high dielectric constant and enhanced energy density. For example, Wen *et al*. revealed that $Ti_{0.87}O_2$ nanosheets are desirable inorganic fillers in poly(vinylidene fluoride) (PVDF) for developing flexible thin-film based capacitor [12]. They successfully incorporated $Ti_{0.87}O_2$ nanosheets into the PVDF matrix through a facile solution casting strategy using NMP as the solvent, which delivers an energy density enhancement of 190% over the bare PVDF. Furthermore, Li *et al*. reported the successful incorporation of $Ca_2Nb_3O_{10}$ nanosheets into ferroelectric PVDF matrix to realize a high energy density of 36.2 J/cm [13]. However, compared with commercial PP, PVDF exhibits high dielectric loss as well as the ferroelectric hysteresis resulting in an energy loss at alternating voltage [14, 15], which significantly restricts its application in high frequency circuits. It is highly desired to incorporate monolayer oxide nanosheets in commercial PP system toward practical application. Unfortunately, the conventional liquid-casting strategy is not viable in commercial PP system due to PP hardly dissolves in any inorganic/organic solvent. The main challenge remains the thin-film fabrication of PP-based polymer/inorganic fillers composites.

Our previous study has realized the application of $Ti_{0.87}O_2$ nanosheets on lithium-ion storage, resistive random access memory (RRAM) and CO_2 electroreduction, respectively [16-18]. In this work, we develop a new strategy including freeze-drying, surface functionalization and hot-pressing to incorporate $Ti_{0.87}O_2$ monolayers in commercial PP film. High-quality colloidal solution consisted of $Ti_{0.87}O_2$ nanosheets with atomic thickness was obtained by a soft-chemical exfoliation route from its layered, protonic precursor. Subsequently, aerogel-like, solid-state $Ti_{0.87}O_2$ nanosheets was freeze-dried from the corresponding single-layer colloidal solution and then surface-modified by coupling agent KH550. Then such an aerogel was successfully embedded in PP matrix with well controllable $Ti_{0.87}O_2$ nanosheets concentration through a hot-pressing strategy (Fig. 1). The resulting $Ti_{0.87}O_2$@PP composited thin-film displayed a remarkable enhancement of 134% on dielectric constant with an optimized $Ti_{0.87}O_2$ concentration of 9 wt%. Our study provides a feasible strategy to embed two-dimensional material into commercial PP thin-film with superior dielectric performance for practical energy-storage application.

2. Experimental

Synthesis of $Ti_{0.87}O_2$ nanosheet colloidal suspension: $Ti_{0.87}O_2$ nanosheets colloidal suspension were prepared via a multistep soft chemical process. In brief, K_2CO_3, Li_2CO_3 and TiO_2 were firstly mixed in a

molar ratio of 2.4 : 0.8 : 10.4, and then heated at 800 ℃ for 30 min to be decarbonated. After cooling, the powder was ground and then calcined at temperatures of 800-1100 ℃ for 20 h to obtain $K_{0.8}Ti_{1.73}Li_{0.27}O_4$. Then this layered alkali metal titanate was mixed with 1 M HCl solution and stirred for several days to be converted into $H_{1.07}Ti_{1.73}O_4{\cdot}nH_2O$. In this step, the solution-to-solid ratio was 100 mL/g, and the acid solution was replaced daily with a fresh one by decantation. A degree of removal of alkali metal ions was studied by chemical analysis. The product was collected by filtration and washed with copious quantities of water. Next, the obtained $H_{1.07}Ti_{1.73}O_4{\cdot}nH_2O$ was further ion-exchanged with 0.1 M tetrabutylammonium hydroxide (TBAOH) at a solution-to-solid ratio of 100 g/mL and then shaken for 7 days, which also led to the osmotic swelling. After exfoliation by ultrasonic, well-dispersed unilamellar nanosheets of $Ti_{0.87}O_2$ were obtained as a stable colloidal suspension.

Preparation of freeze-dried aerogel and surface-modified $Ti_{0.87}O_2$ nanosheets: 100 ml $Ti_{0.87}O_2$ nanosheets colloidal solution with a concentration of 4.0 g/L was added in a 300 ml beaker and then freeze-dried in the freeze dryer for 4 days. Afterwards, loose gel-like sample with a cotton-like shape can be directly obtained. The KH550 modification process of freeze-dried $Ti_{0.87}O_2$ was as follows. First, 2 ml silane coupling agent KH550 was dispersed in 5 ml ethanol. Then 3 g freeze-dried $Ti_{0.87}O_2$ nanosheets and KH550/ethanol mixture were added together into 10 ml ethanol. After being stirred for 24 h, the mixture was centrifuged at 10000 rpm for 5min to collect the white slurry at the bottom of the tube and washed by ethanol three times to remove the excess KH550. The product was then dried in the oven at 60 ℃ for 12 h and the white KH550 modified freeze-dried $Ti_{0.87}O_2$ powder can be obtained.

Preparation of $Ti_{0.87}O_2$@PP composite film: PP particles (melt flow rate 3.2 g/10 min) were purchased from Borealis and the xylene (AR) was purchased from Aladdin. To homogeneously blend the as-prepared $Ti_{0.87}O_2$ and PP particles, firstly, PP particles were ball milled into powder form as follows: 10 g PP commercial particles and 100 ml xylene were added in a 400 ml beaker and heated in oil bath at 140 ℃. Until PP particles dissolved completely, the uniform solution was placed at room temperature for 2 days to volatilize xylene. The resulting white PP block by this treatment was cut to small pieces. 3 g PP pieces and grinding medium (steel balls of different diameter, 5, 10, and 20 mm, with a weight ratio of 7:2:1 in sequence) were put into a 50 ml sealed agate jar and milled in a high-energy planetary ball mill system with an autorotation speed of 400 rpm at room temperature for 2 h. Then the ball-milled powders were passed through an 80-mesh sieve. The screened PP powders and as-prepared $Ti_{0.87}O_2$ were mixed in different weight ratio of $Ti_{0.87}O_2$ (0%, 3%, 6%, 9%, 12%, 15%) and milled with an autorotation speed of 600 rpm at room temperature for 4 h. The well mixed powder was heated at 180 ℃ for 15 min without pressure and then kept at 180 ℃ under 12 MPa for 15 min in the press vulcanizer. Upon cooling to room temperature, the $Ti_{0.87}O_2$@PP composite film was removed from the plate for further analysis.

Materials characterization

The phase structure was characterized by a Bruker D8-A25 diffractometer using Cu Kα radiation (λ = 1.5406 Å). Sample morphologies were characterized using a FEI Navo Nano SEM 450 field-emission

scanning electron microscope (SEM) and a Bruker Dimension Icon atomic force microscope (AFM). Transmission electron microscopy (TEM) and selected area electron diffraction (SAED) were performed using a Philips CM 200 FEG field emission microscope at an acceleration voltage of 300 kV.

Dielectric measurement

The dielectric properties of the composite samples were measured using LRC digital bridge (HIOKI IM3533) in the frequency range of 10 Hz to 100 kHz. Prior to measurement, a thin cover of the silver paste was coated on the two sides of all samples. The electrical breakdown test was carried out via high voltage DC generator (ZGF-120/2). The generator applies an increasing voltage on the sample until the sample breakdown. Multimeter (MASTECH MY65) is used to measure the voltage of the sample. We carried out the electrical breakdown test three times on each sample and the real data is the average value of three measurements.

3. Results And Discussion

Firstly, titanate precursor ($K_{0.8}Ti_{1.73}Li_{0.27}O_4$) was obtained by a solid-state calcination process, and protonic $H_{1.07}Ti_{1.73}O_4 \bullet nH_2O$ bulk was prepared from $K_{0.8}Ti_{1.73}Li_{0.27}O_4$ by acid exchange as previously reported (Fig. 2a) [19]. Then 2D $Ti_{0.87}O_2$ nanosheets with atomic thickness were obtained by a liquid-exfoliation strategy from the layered $H_{1.07}Ti_{1.73}O_4 \bullet nH_2O$ precursor with an aqueous solution of tetrabuthylammonium hydroxide (TBAOH) [20]. After the soft-chemical exfoliation, highly stable, transparent colloidal suspension of $Ti_{0.87}O_2$ nanosheets exhibits a clear Tyndall light scattering (Fig. 2b). As demonstrated by the atomic force microscopy (AFM) characterization, the thickness of the $Ti_{0.87}O_2$ nanosheets is approximately 2-3 nm (Fig. 2c-d). The transmission electron microscopy (TEM) images exhibit two-dimensional ultrathin sheets with lateral dimensions up to 4 μm while fragments and folded edges were also observed in small amounts (Fig. 2e-f). The SAED pattern taken from the aggregation of several sheets exhibits polycrystalline diffraction rings (Fig. 2g).

$H_{1.07}Ti_{1.73}O_4 \bullet nH_2O$ and the corresponding crystallographic structure. (b) The as-prepared colloidal suspension of $Ti_{0.87}O_2$ nanosheets with a typical Tyndall effect (concentration: 0.2 g/L). (c, d) Tapping-mode AFM image and the height information of the as-exfoliated nanosheets. (e, f) TEM images and (g) SAED pattern of the aggregation of $Ti_{0.87}O_2$ nanosheets.

Considering that PP matrix is insoluble in most of organic/inorganic solvent, it is necessary to recover our $Ti_{0.87}O_2$ nanosheets from the colloidal suspension and then embed it into PP through a non-solution based strategy. We used the freeze-drying technique to obtain the aerogel sample of the atomically flat $Ti_{0.87}O_2$ nanosheets. After freeze-dried of the colloidal solution with a concentration of 4.0 g/L in vacuum for 4 days, white, loose aerogel-like sample with a cotton-like shape was obtained as shown in Fig. 3a. A set of sharp diffraction lines indexed as 0k0 (k = 1, 2, 3, 4, 5) diffraction peaks can be detected in the corresponding XRD pattern (Fig. 3b). The basic d-spacing of (010) peak is estimated to be 1.73 nm, which is indicative of a lamellar structure with a gallery height of 1.73 nm. SEM observation further confirms

that the freeze-dried product is consisted of numerous thin-flakes with curved edges and a thickness of 20-30 nm (Fig. 3c-d), suggesting that about 10-15 atomically thin nanosheets were restacked along [00*l*] direction during the freeze-drying process. Note that such a thickness is also drastically smaller than that of pristine layered $H_{1.07}Ti_{1.73}O_4 \bullet nH_2O$ bulk, leading to a large aspect ratio of more than 100.

Subsequently, the freeze-dried $Ti_{0.87}O_2$ aerogel were used as the inorganic fillers embedded in PP matrix to fabricate composited thin-film through a hot-pressing process. We found that commercial PP particles are hardly ball-milled directly into powder form. However, dissolution PP particles in xylene at 140 ℃ and cooled down to room temperature results in the recrystallization of PP, which can be ball-milled into powder easily. After the hot-pressing of the freeze-dried $Ti_{0.87}O_2$ aerogel and the ball-milled PP powder into a composite thin-film, the characteristic (*0k0*) peaks of $Ti_{0.87}O_2$ disappeared (Fig. 4a). We considered that it should be attributed to the drastic aggregation of the $Ti_{0.87}O_2$ aerogel in PP matrix. Such a problem has been successfully solved by the surface modification using coupling agent KH550 in ethanol. After such a pretreatment, the $Ti_{0.87}O_2$ nanosheets still maintain a layered crystal structure (Fig. 4b) and (010) peaks can be clearly detected from the composited thin-film as shown in Fig. 4c-d. We further confirm the uniformity of this composited film by recording the XRD patterns from four distinct positions on the surface of this nanocomposite film. As shown in Fig. 4f, these four positions 1-4 show analogous XRD patterns with the appearance of (010) peaks from our $Ti_{0.87}O_2$ fillers. This result demonstrates that $Ti_{0.87}O_2$ fillers are homogeneously dispersed in PP polymer.

Fig. 5 show the characteristic scanning electron microscopy (SEM) images of the resulting $Ti_{0.87}O_2$@PP composite films with various concentration of KH550/$Ti_{0.87}O_2$ nanosheet fillers from 0 wt% to 15 wt%. One can see that KH550/$Ti_{0.87}O_2$ nanosheet fillers are well dispersed in PP matrix without any accumulation until the concentration up to 9% (Fig. 5a-d). However, the agglomeration of $Ti_{0.87}O_2$ flakes with size of 500-1000 nm can be observed when its concentration up to 12-15 wt% (Fig. 5e-f).

The dielectric constant (ε_r) of $Ti_{0.87}O_2$@PP composite films at different frequencies is shown in Fig. 6a. It can be seen a downward trend of dielectric constant in low frequency (<10^3 Hz) in all of the $Ti_{0.87}O_2$@PP composite films, and such a downward trend generally become stable in high frequency range (>10^3 Hz). This result implies excellent compatibility between KH550 treated $Ti_{0.87}O_2$ and pure PP matrix. The dielectric constant of the hybrid film with different $Ti_{0.87}O_2$ concentrations at 10^3 Hz is given in Fig. 6b. The dielectric constant increases with $Ti_{0.87}O_2$ weight fraction to a maximum of 3.27 at 9 wt%, which is 134% higher than pure PP film prepared through the same method. Such a result is attributed to the giant dielectric constant of $Ti_{0.87}O_2$ originated from the existence of abundant Ti vacancies which act as carrier traps and high-leakage paths [10]. However, further increase of the $Ti_{0.87}O_2$ content than this threshold value of 9 wt% leads to a steady decrease in the dielectric constant. This phenomenon is thought to be caused by accumulation of the nanosheets at high weight fraction of $Ti_{0.87}O_2$ filler. Fig. 6c shows the dielectric loss of all $Ti_{0.87}O_2$@PP composites at different frequencies. The dielectric loss tangent increases to the maximum value when the concentration of $Ti_{0.87}O_2$ filler is 9 wt%, well consistent with

the result in Fig. 6a. The breakdown field (E) trend of a series of $Ti_{0.87}O_2$@PP composite film in Fig. 6c suggests that the increase of dielectric constant leads to a decrease in dielectric strength of the composited thin-film. An important reason should be the nanosheets incorporated in PP may induce space void at the $Ti_{0.87}O_2$ nanosheet/ PP matrix interface. Note that such a decrease is much lower than that of the thin-film fabricated by solution-based method (E = 33 MV/m) as reported previously [21]. The superior property should benefit from the large aspect ratio of our $Ti_{0.87}O_2$ nanosheets fillers, which may act as barrier for relieving the diffusion of electrical tree, then restraining the avalanche of electric breakdown as a result [22].

4. Conclusion

In summary, we successfully developed a new strategy including freeze-drying, surface functionalization and hot-pressing to incorporate $Ti_{0.87}O_2$ monolayers in PP film. The $Ti_{0.87}O_2$ nanosheets were firstly freeze-dried into aerogel form and surface modified by KH550 coupling agent, and such an aerogel was successfully embedded in PP matrix with well controllable $Ti_{0.87}O_2$ nanosheets concentration through a hot-pressing strategy. XRD and SEM characterizations of the $Ti_{0.87}O_2$@PP composite film demonstrate that the $Ti_{0.87}O_2$ fillers are uniformly dispersed in the PP matrix. The dielectric constant of the $Ti_{0.87}O_2$@PP composite film exhibits maximum value of 3.27 when the $Ti_{0.87}O_2$ content is 9 wt%, which is about 1.5 times higher than that of pure PP film. Our study provides a feasible approach to embed two-dimensional material into commercial PP thin-film with high dielectric constant for practical energy-storage applications.

Declarations

Acknowledgements

This work was financially supported by the Researching Program of State Grid Corporation of China (GYW17201800011).

Reference

[1] Li Q, Chen L, Gadinski MR, *et al*. Flexible high-temperature dielectric materials from polymer nanocomposites. *Nature* 2015, **523**: 576-579.

[2] Yao Z, Song Z, Hao H, *et al*. Homogeneous/Inhomogeneous-structured dielectrics and their energy-storage performances. *Adv Mater* 2017, **29**: 1601727.

[3] Dang ZM, Yuan JK, Zha JW, *et al*. Fundamentals, processes and applications of high-permittivity polymer-matrix composites. *Prog Mater Sci* 2012, **57**: 660-723.

[4] Luo SB, Yu JY, Yu SH, *et al*. Significantly enhanced electrostatic energy storage performance of flexible polymer composites by introducing highly insulating- ferroelectric microhybrids as fillers. *Adv Energy Mater* 2019, **9**: 1803204.

[5] Pan ZB, Yao LM, Zhai JW, *et al*. Interfacial coupling effect in organic/inorganic nanocomposites with high energy density. *Adv Mater* 2018, **30**: 1705662.

[6] Qiao YL, Yin XD, Zhu TY, *et al*. Dielectric polymers with novel chemistry, compositions and architectures. *Prog Polym Sci* 2018, **80**: 153-162.

[7] Zhang Y, Zhang CH, Feng Y, *et al*. Excellent energy storage performance and thermal property of polymer-based composite induced by multifunctional one-dimensional nanofibers oriented in-plane direction. *Nano Energy* 2019, **56**: 138-150.

[8] Luo H, Zhou XF, Ellingford C, *et al*. Interface design for high energy density polymer nanocomposites. *Chem Soc Rev* 2019, **48**: 4424-4465.

[9] Zheng MS, Zha JW, Yang Y, *et al*. Polyurethane induced high breakdown strength and high energy storage density in polyurethane/poly(vinylidene fluoride) composite films. *Appl Phys Lett* 2017, **110**: 252902.

[10] Osada M, Ebina Y, Funakuba H, *et al*. High-κ dielectric nanofilms fabricated from titania nanosheets. *Adv Mater* 2006, **18**: 1023-1027.

[11] Osada M, Sasaki T. Two-dimensional dielectric nanosheets: novel nanoelectronics from nanocrystal building blocks. *Adv Mater* 2012, **24**: 210-228.

[12] Wen RM, Guo JM, Zhao CL, *et al*. Nanocomposite capacitors with significantly enhanced energy density and breakdown strength utilizing a small loading of monolayer titania. *Adv Mater Interfaces* 2018, **5**: 1701088.

[13] Bao ZW, Hou CM, Shen ZH, *et al*. Negatively charged nanosheets significantly enhance the energy-storage capability of polymer-based nanocomposites. *Adv Mater* 2020: 1907227.

[14] Yang LY, Ho J, Allahyarov, E, *et al*. Semicrystalline structure-dielectric property relationship and electrical conduction in a biaxially oriented poly(vinylidene fluoride) film under high electric fields and high temperatures. *ACS Appl Mater Interfaces* 2015, **7**: 19894.

[15]Huan TD, Boggs S, Teyssedre G, *et al*. Advanced polymeric dielectrics for high energy density applications. *Prog Mater Sci* 2016, **83**: 236.

[16] Dai R, Zhang AQ, Pan ZC, *et al*. Epitaxial growth of lattice-mismatched core-shell TiO_2@MoS_2 for enhanced lithium-ion storage. *Small* 2016, **12**: 2792-2799.

[17] Dai YW, Bao WZ, Hu LF, *et al*. Forming free and ultralow-power erase operation in atomically crystal TiO_2 resistive switching. *2D Mater* 2017, **4**: 025012.

[18] Han P, Wang ZJ, Kuang M, *et al*. 2D assembly of confined space toward enhanced CO_2 electroreduction. *Adv Energy Mater* 2018, **8**: 1801230.

[19] Sasaki T, Kooli F, Iida M, *et al*. A mixed alkali metal titanate with the lepidocrocite-like layered structure. Preparation, crystal structure, protonic form, and acid-base intercalation properties. *Chem Mater* 1998, **10**: 4123-4128.

[20] Sasaki T, Nakano S, Yamauchi S, *et al*. Fabrication of titanium dioxide thin flakes and their porous aggregate. *Chem Mater* 1997, **9**: 602-608.

[21] Hidayah IN, Mariatti M, Ismail H, *et al*. Evaluation of PP/EPDM nanocomposites filled with SiO_2, TiO_2 and ZnO nanofillers as thermoplastic elastomeric insulators. *Plast Rubber Compos* 2015, **44**: 259-264.

[22] Dang ZM, Yuan JK, Yao SH, *et al*. Flexible nanodielectric materials with high permittivity for power energy storage. *Adv Mater* 2013, **25**: 6334-6365.

Figures

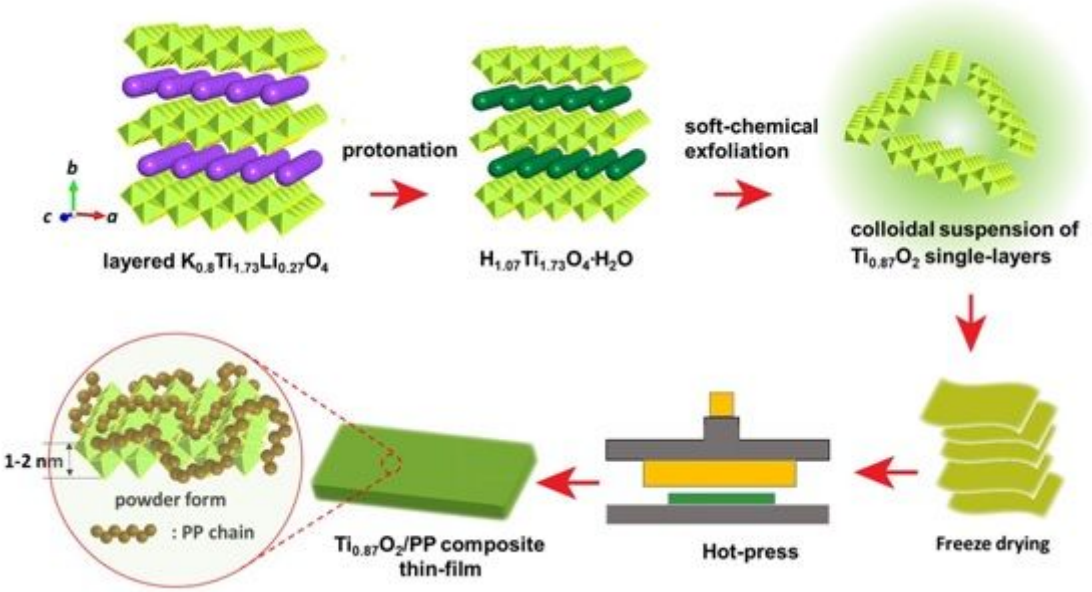

Figure 1

Schematic illustration of the strategy for the Ti0.87O2@PP composited thin-film fabrication.

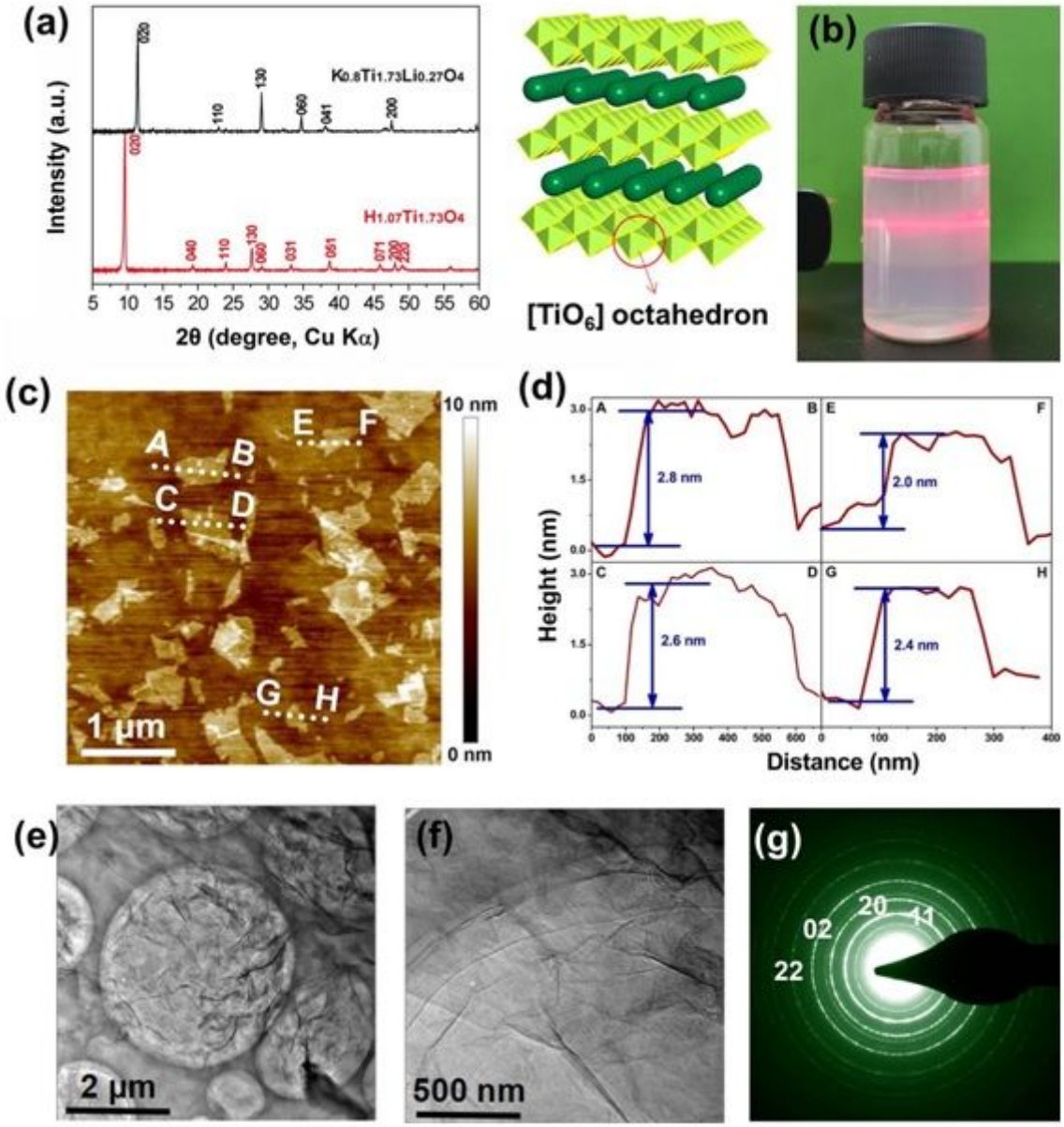

Figure 2

(a) XRD powder pattern of layered K0.8Ti1.73Li0.27O4 precursor, the protonated H1.07Ti1.73O4•nH2O and the corresponding crystallographic structure. (b) The as-prepared colloidal suspension of Ti0.87O2 nanosheets with a typical Tyndall effect (concentration: 0.2 g/L). (c, d) Tapping-mode AFM image and the height information of the as-exfoliated nanosheets. (e, f) TEM images and (g) SAED pattern of the aggregation of Ti0.87O2 nanosheets.

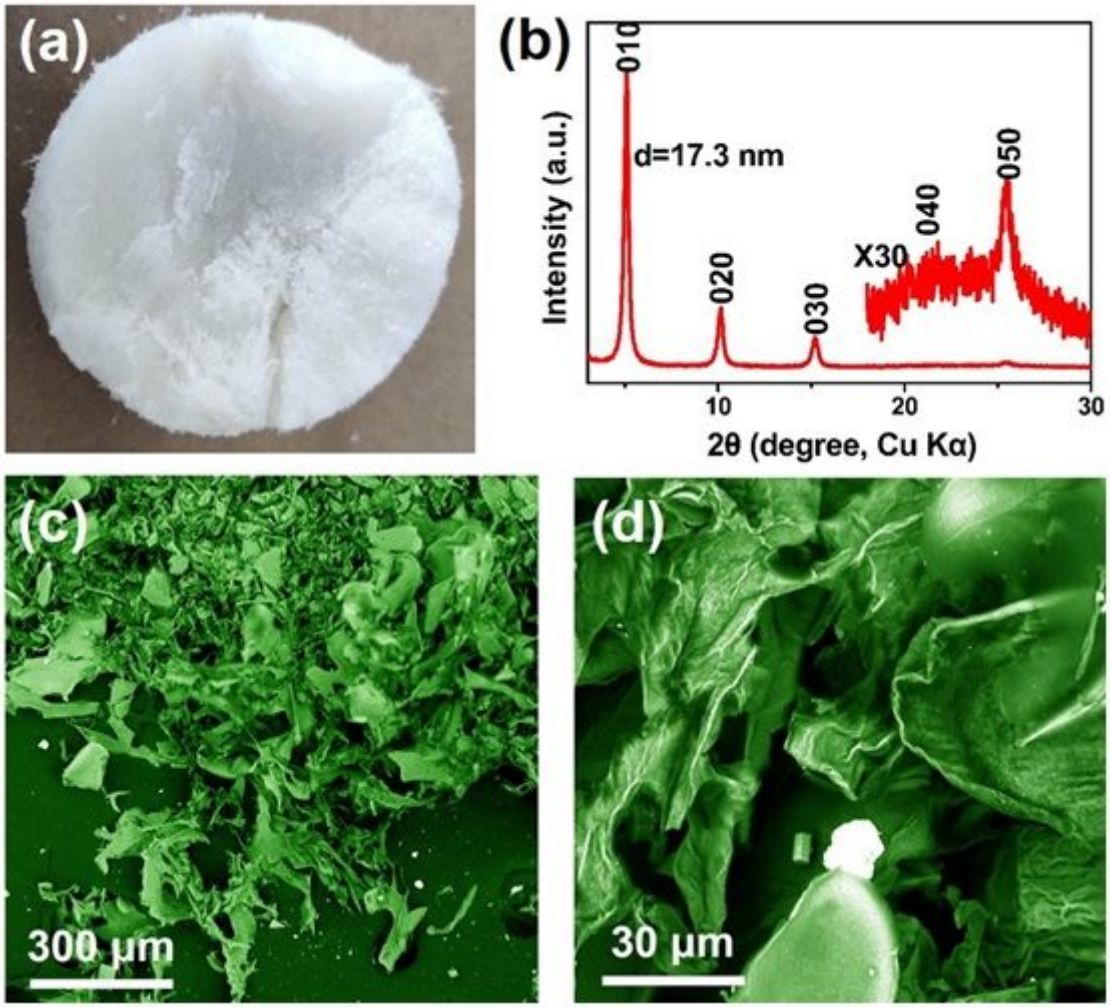

Figure 3

(a) Photograph of the freeze-dried aerogel sample obtained from the colloidal suspension of Ti0.87O2 nanosheets. (b) XRD pattern of the freeze-dried Ti0.87O2 aerogel. Inset is the enlarged view of the XRD pattern in higher angles. (c, d) The corresponding SEM images with different magnifications.

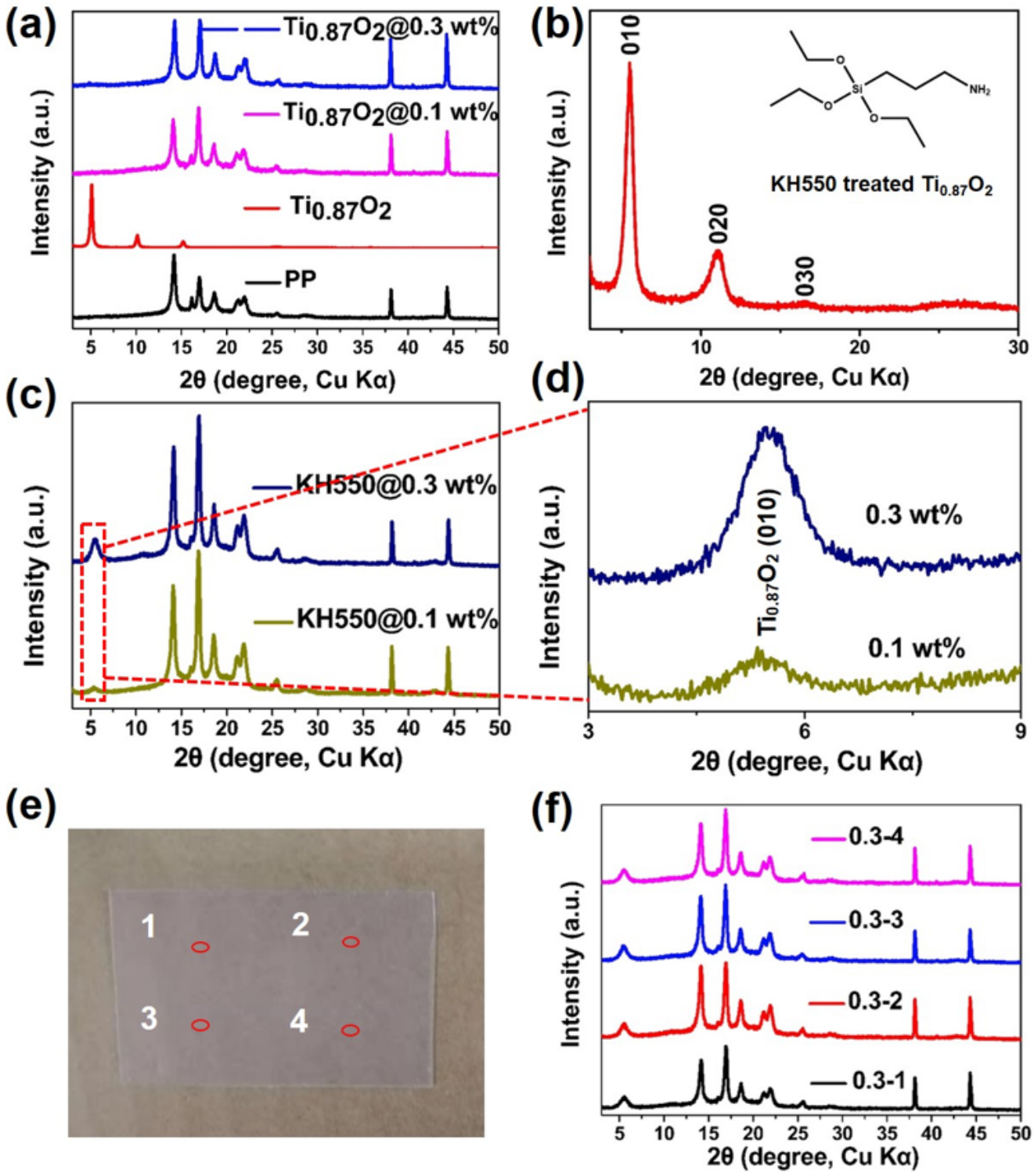

Figure 4

(a) XRD patterns of PP, freeze-dried Ti0.87O2 and the Ti0.87O2@PP composite film at various weight fraction of Raw Ti0.87O2. (b) XRD patterns of KH550 treated Ti0.87O2 and molecular structural formation of the coupling agent KH550. (c) XRD patterns of Ti0.87O2@PP composite at various weight fraction of Ti0.87O2 treated with KH550. (d) The XRD peaks of the (010) plane of KH550 treated

Ti0.87O2 (e, f) Photograph of the 0.3 wt% KH550 treated Ti0.87O2@PP composite film and XRD patterns recorded from four different points of the composite film.

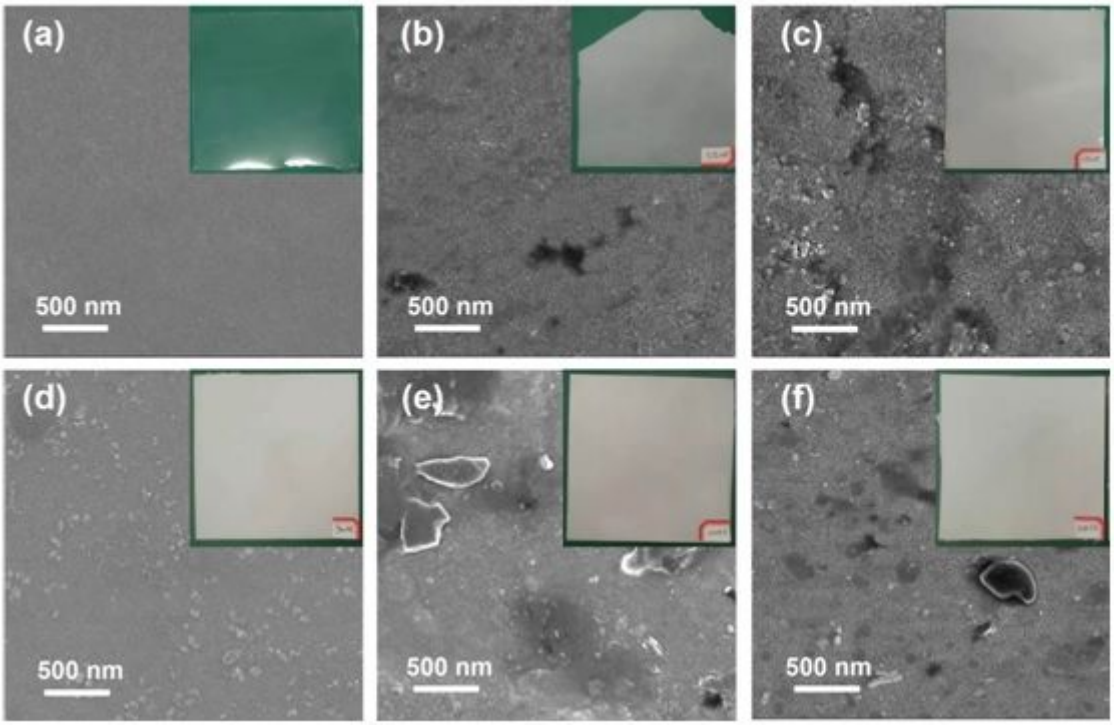

Figure 5

The SEM images and photographs of (a) pure PP, KH550 modified Ti0.87O2@PP composited thin-film with various weight fraction of (b) 3%, (c) 6%, (d) 9%, (e) 12%, (f) 15%.

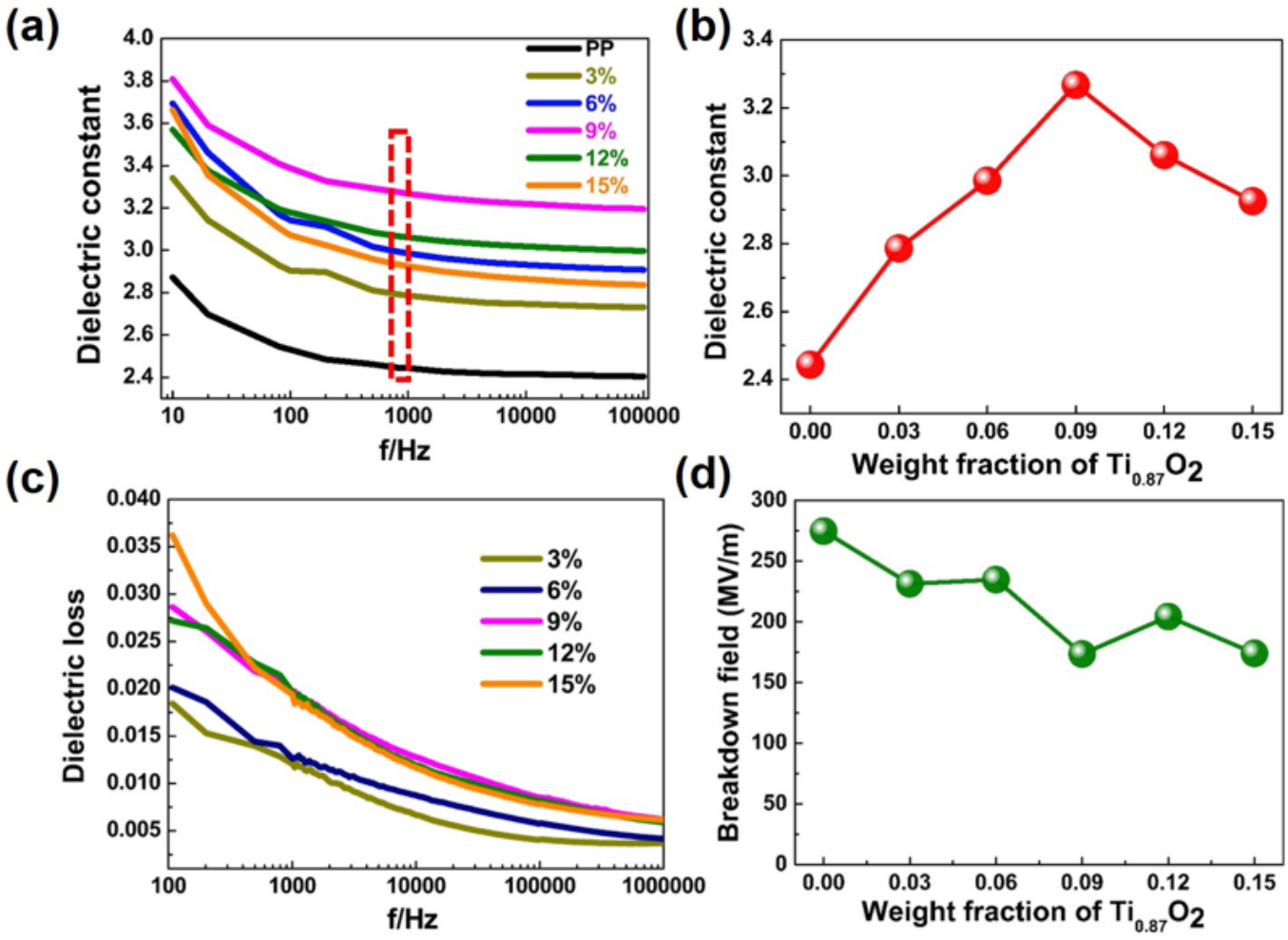

Figure 6

Dielectric properties of Ti0.87O2@PP composite film with different concentration of KH550 treated Ti0.87O2. (a) The frequency dependence of dielectric constant. (b) The dielectric constant in 1 kHz. (c) The frequency dependence of dielectric loss. (d) The curves of breakdown field.